Intensified adsorption of cesium by PVDF-g-caffeic acid/Prussian blue/polytetrafluoroethylene sandwich membranes

Shuang Hao, Zhiqian Jia*

Lab for Membrane Science and Technology, College of Chemistry, Beijing Normal University, Beijing 100875, China, emails: zhqjia@bnu.edu.cn (Z. Jia), sherily-Haos@bnu.edu.cn (S. Hao)

A B S T R A C T

Membrane adsorption has emerged as a novel technology for the adsorption of trace substances. To intensify the membrane adsorption of cesium (Cs^+), Prussian blue (PB) nanoparticles were synthesized by Fe(III)-oxalic acid complex conversion, and caffeic acid (CA) was grafted onto poly(vinylidene fluoride) (PVDF). Then, the PVDF-g-CA/PB/polytetrafluoroethylene sandwich membranes were fabricated by filtration/nonsolvent vapor-induced phase separation for the first time. The effects of air humidity, polymer concentrations, and PB contents on the membrane morphology, flow rates and adsorption capacity were studied, and a series-resistance model was employed to describe the hydrodynamic resistances of the membranes. The results show that under optimized fabrication conditions, the maximum adsorption capacity of the membranes is 1.12 mmol m^{-2} for Cs^+, and the selectivity of Cs^+ vs. Li^+, Na^+ and K^+ is 44.31, 15.38 and 27.33, respectively. The adsorption isotherm of Cs^+ can be well described by the Langmuir model. The membrane resistance increases with increasing polymer concentrations and PB contents. The sandwich membranes exhibit excellent dynamic adsorption performance and reusability, indicating great potential for the adsorption of Cs^+.

Keywords: Prussian blue; Sandwich membrane; Adsorption; Cesium; Caffeic acid

1. Introduction

Cesium (Cs) is an alkali metal that is widely used in scintillation detectors, photocells, catalysts, healthcare, etc. [1,2]. Salt lake brines are important Cs sources, in which trace Cs coexists with other alkali metals, that is, lithium, sodium and potassium [3]. Various methods, such as electrocoagulation [4], ion exchange [5], adsorption [6–10] and electrochemical separation [11], have been employed for the separation of Cs^+. Among these techniques, adsorption is cost-effective and easy to operate. Grafted catechol [12], clay minerals [13], resorcinol formaldehyde [14] and Prussian blue (PB) [15] have been employed as adsorbents. PB possesses hydrophilic defect cages and can trap Cs^+ ions selectively with high capacity [15,16]. Nevertheless, PB powders are usually ultrafine, resulting in high resistance in the adsorption bed. Thus, immobilizing PB on a porous support or incorporating it into a polymer matrix is widely employed [17,18].

Membrane adsorption has emerged as a novel technology in recent years, especially for the adsorption of trace substances. Adsorptive membranes are usually prepared by incorporating nano- or microsized adsorbents in a polymer matrix [19,20], referred as mixed matrix membranes (MMMs). However, the low loading and encapsulation of powders by the matrix often lead to low adsorption capacity and slow adsorption rate. Adsorptive membranes with adsorbents grown on membrane surface [18], or adsorbents sandwiched between substrate membrane and surface membrane formed

* Corresponding author.

through non-solvent immersion-induced phase separation (NIPS) [21,22] were also reported.

To further intensify the membrane adsorption process, in the present study, PB nanoparticles were synthesized by the Fe(III)-oxalic acid complex conversion method, and caffeic acid (CA) was grafted on poly(vinylidene fluoride) (PVDF). Then, the PVDF-g-CA/PB/polytetrafluoroethylene sandwich membranes were fabricated by the filtration/non-solvent vapor-induced phase separation (VIPS) method for the adsorption of Cs^+ for the first time. Caffeic acid (CA) possesses catechol groups and can adsorb Cs^+, and polytetrafluoroethylene (PTFE) displays excellent chemical and thermal stability [23] and acts as a robust substrate. The VIPS method favors the formation of PVDF-g-CA membranes with large pores. Furthermore, in the fabrication, the PVDF-g-CA solution can penetrate the micropores of the PTFE margin and act as anchors, enhancing the integrated strength and stability of the sandwich membranes. The effects of air humidity, polymer concentrations and PB contents on the membrane morphology, flow rates and adsorption capacity were studied, and a series-resistance model was employed to describe the hydrodynamic resistances of the membranes.

2. Experimental

2.1. Materials

Benzophenone (BP, 98%), CsCl, RbCl, KCl, NaCl, LiCl, NH_4Cl, HCl, ethanol, N,N′-dimethylformamide (DMF), $K_4Fe(CN)_6$, $FeCl_3$, oxalic acid and caffeic acid (CA) were analytical grade, provided by the Beijing Chemical Factory (Beijing, China) and used as received without further purification. PVDF 6008 (Mw = 20,000) was purchased from the Solvay Company, and PTFE microfiltration membranes (Φ50 mm, pore size of 0.10 μm) were provided by the Haining Chuangwei Filtration Equipment Factory, China.

2.2. Preparation of PB

PB particles were synthesized by Fe(III)-oxalic acid complex conversion [24]. Then, 0.06 mol of oxalic acid and 0.002 mol of $FeCl_3$ were mixed in 500 mL of DI water under stirring for 0.5 h, and 20 mL of 0.1 mol/L $K_4Fe(CN)_6$ solution was added and stirred vigorously for 3 h. The obtained precipitates were centrifuged and washed three times with distilled water.

2.3. Preparation of PVDF-g-CA

CA was grafted onto PVDF by a UV preactivation/thermal initiation method [25]. PVDF powder (7 wt%) and BP (5 wt%) were dissolved in 15 mL of DMF, bubbled with N_2 for 15 min, and irradiated with UV rays (high-pressure UV lamp, 700 W) for 40 min. Then, 1 g of caffeic acid was added, bubbled with N_2 for 15 min, heated to 80°C, and reacted for 3 h. Finally, ethanol was added, and the precipitates were centrifuged, extracted in ethanol by a Soxhlet extractor for 3 d, washed five times with ethanol and dried until constant weight. A certain amount of PVDF-g-CA was dissolved in DMF to obtain PVDF-g-CA solution.

2.4. Fabrication of sandwich adsorptive membranes

PVDF-g-CA/PB/PTFE membranes were prepared by the filtration/VIPS method [26,27]. The PB dispersion in DI water was filtrated by PTFE microfiltration membrane. Then, the PVDF-g-CA solution was cast on PB/PTFE using a knife (spacing of 700 μm) and then maintained in a constant temperature and humidity chamber (HSX-350, Shanghai Fuma Company, Shanghai, China) for 6 h for phase inversion. With the penetration of water vapor into the wet membrane as well as the evaporation of DMF, porous PVDF-g-CA membranes formed. For comparison, MMMs were also prepared by casting PVDF-g-CA solution containing PB on the PTFE substrate, and then maintained under a certain humidity and temperature for 6 h for phase inversion.

2.5. Adsorption

The static adsorption experiments were carried out in a conical flask at 25°C (pH = 7) under shaking for 24 h. The adsorption capacity (Q_e, mmol/g) is calculated as follows:

$$Q_e = \frac{(c_0 - c_e) \times v_0}{w_0} \tag{1}$$

where c_0 and c_e are the initial and equilibrium metal ion concentration (mmol/L), respectively, v_0 is the solution volume (L), w_0 is the membrane mass (g). The selectivity factor is defined as $Q_{e,i}/Q_{e,j}$, where i and j represent cation i and j, respectively.

In the dynamic adsorption experiments, the membranes (diameter of 50 mm) were first preconditioned with 3 × 5 mL of water. Then, 300 mL of alkali aqueous solution flowed through the membranes at a rate of 3.33 mL/min, and the filtrate was collected at intervals for analysis.

2.6. Characterization

The morphology of the membranes was characterized by field emission scanning electron microscopy (S-8010, Hitachi Japan, EDS, XFlash 6160, BRUKER, Germany). The alkali metal concentrations were determined by inductively coupled plasma mass spectrometry (ICP-MS, NexION300x, PerkinElmer Instruments Co., Ltd.). The grafting degree of PVDF was determined by the carbonyl index [28], which is defined as the ratio of IR absorbance of carbonyl (at 1,720 cm^{-1}, A_{1720}) to that of C–F (at 1,160 cm^{-1}, A_{1160}, as the reference).

$$CI = \frac{A_{1720}}{A_{1160}} \tag{2}$$

3. Results and discussion

3.1. Preparation of PB and PVDF-g-CA

The powder X-ray diffraction (PXRD) pattern of the PB particles shows peaks at 17.5°, 24.8°, 35.4°, 39.8°, 43.7°, 50.9° and 54.3°, corresponding to the 200, 220, 400, 420, 422, 440, 600 and 620 crystal planes, which is consistent with the literature [29]. The SEM analysis presents uniform PB particles, approximately 200 nm in size (Fig. 1).
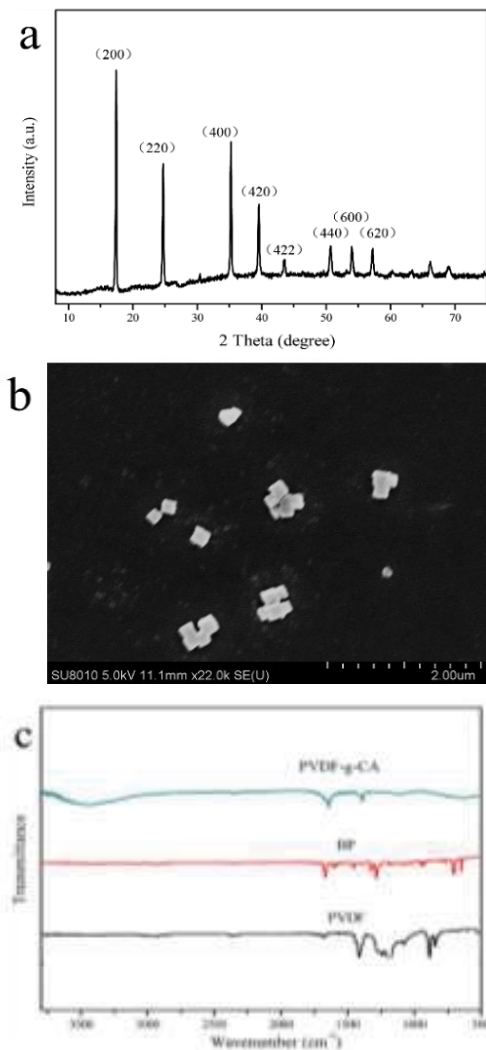
FIG. 1. Characterization of PB particles and PVDF-g-CA. (a) PXRD of PB particles. (b) SEM image of PB. (c) FTIR of PVDF-g-CA.

For the preparation of PVDF-g-CA, the excited BP abstracts hydrogen from PVDF and generates PVDF radicals, and BP is reduced to semipinacol radicals [30]. PVDF radicals and semipinacol radicals combine and form PVDF initiators in the absence of CA. In thermal initiation grafting, CA was added, and heating leads to the decomposition of PVDF initiators into PVDF radicals and semipinacol radicals, and then the PVDF radicals initiate the CA grafting. The carbonyl index of the obtained PVDF-g-CA was 2.88, indicating the successful grafting of CA onto PVDF [25].

3.2. Fabrication of sandwich membranes

3.2.1. Effects of relative humidity

The filtration/VIPS method was employed for the fabrication of PVDF-g-CA/PB/PTFE membranes. To explore the effects of relative humidity (RH) on the membranes, the PB (0.075 g) dispersion was filtered by a PTFE microfiltration membrane, and the PVDF-g-CA/PVDF DMF solution

(containing 10 wt% of PVDF-g-CA and 4 wt% PVDF, in which PVDF was used to enhance the membrane stability in water) was cast onto PB/PTFE using a knife and then maintained under a certain humidity (20%, 40%, 60% and 80% RH) at 25°C for 6 h.

Fig. 2 shows that for 20%, 40%, 60% and 80% RH, the surface pores of the membranes are approximately 1, 2, 4 and 2 μm in average size, respectively. A cross-section of the membranes shows that the respective thicknesses of the PTFE, PB and PVDF-g-CA/PVDF layers are approximately 340, 40 and 40 μm, respectively. When the humidity is low (20% and 40% RH), solvent evaporation is the dominant mechanism for membrane formation, and small pore sizes and dense membrane structures form. At high humidity (60% RH), membrane formation is dominated by water vapor penetration-induced phase separation, leading to large pore sizes and loose membrane structures [31]. When the humidity is too high (80% RH), the penetration of water vapor into the wet membrane is very fast, leading to rapid phase separation and thus small pore sizes [32]. The breath figure patterns are just kinetic effect but rather the thermodynamic equilibrium state, leading to not obvious change of membrane surface morphology under various humidity [33]. Due to the limited non-solvent in water vapor and the slow phase separation, the cross-section of membranes finally forms a symmetrical structure, avoiding the formation of hole defects in NIPS method.

The flow rates of Cs^+ solution through the above PVDF-g-CA/PB/PTFE membranes at 0.08 MPa are 0.48, 3.91, 5.48 and 4.81 mL/min (Fig. 3a), which is in good agreement with the membrane pore sizes. The flow rates through the PTFE substrate and PVDF-g-CA/PTFE membrane (obtained at 60% RH) at 0.08 MPa were also measured and were found to be 100 and 28.44 mL/min, respectively. In the filtration process, the flux can be expressed with the series-resistance model [34],

$$J_v = \frac{\Delta p}{\mu(R_a + R_b + R_c)} \tag{3}$$

where J_v is the flux (L/(m^2 h)), Δp is the pressure difference (MPa), and R_a, R_b and R_c are the respective resistances of PTFE, PB and PVDF-g-CA/PVDF layers (m^{-1}).

From Eq. (1), it was found that the overall resistances of the sandwich membranes are 19.63×10^{12}, 2.41×10^{12}, 1.72×10^{12} and 1.96×10^{12} m^{-1} (Fig. 3a), and the resistances of the PTFE and PB layers are 1.2×10^{11} and 1.4×10^{12} m^{-1}. As the relative humidity only affects the structure of the PVDF-g-CA/PVDF layer, the resistances of the PTFE and PB layers can be considered constant; the PVDF-g-CA resistances are 18.13×10^{12}, 9.1×10^{11}, 2.2×10^{11} and 4.5×10^{11} m^{-1}, approximately 92%, 38%, 13% and 23% of the total resistance, respectively. Clearly, the small pore sizes and the dense structure of the PVDF-g-CA/PVDF layer lead to high resistance. Considering the hydrodynamic resistance, hereafter, 60% RH (25°C) was used for the preparation of the sandwich membranes.

3.2.2. Effects of the polymer concentration

The effects of the polymer concentration (10%, 12%, 14%, 16% and 18%, including 10% PVDF-g-CA and 0%, 2%,
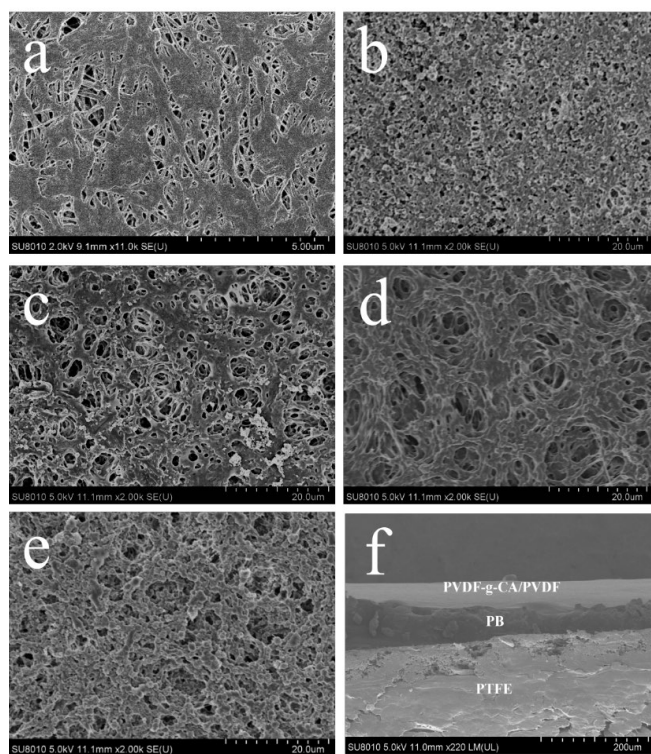
Fig. 2. Effects of relative humidity on membranes. (a) Surface of PTFE substrate. (b) Surface of membrane prepared under 20% RH. (c) Surface of membrane prepared under 40% RH. (d) Surface of membrane prepared under 60% RH. (e) Surface of membrane prepared under 80% RH. (f) Cross-section of membrane. As the PTFE substrate is very thick, and the SEM image only shows part of the PTFE.

4%, 6% and 8% PVDF, respectively) on the membranes were studied at a constant PB content of 0.075 g and 60% RH. With increasing polymer concentrations, the flow rates of Cs⁺ solution under 0.08 MPa decrease apparently (15.48, 10.92, 5.48, 3.04 and 2.16 mL/min) (Fig. 3b), and the overall membrane resistance and the surface membrane resistance increase, and the surface resistance ratio rises from 3% to 10%, 13%, 52% and 66% of the overall resistance. The reason is ascribed to the increased thickness and density of surface membrane layer in term of the polymer concentration and the surface resistance ratio. When the polymer concentration exceeds 14%, the thickness and resistance of the surface layer quickly increase. Therefore, 14% polymer was used as the optimized concentration.

3.2.3. Effects of the PB contents

The effects of the PB contents were explored under a polymer concentration of 14% (10% PVDF-g-CA and 4% PVDF), with 60% RH, and PB contents of 0.0125, 0.025, 0.05 and 0.075 g. With the increased PB contents, the flow rate of Cs⁺ solutions through the membranes under 0.08 MPa decreases from 28.44 to 13.34, 8.66, 6.24 and 5.48 mL/min (Fig. 3c), and the total membrane resistance increases from 0.33×10^{12} to 0.71×10^{12}, 1.09×10^{12}, 1.51×10^{12} and 1.72×10^{12} m⁻¹, and the PB layer resistance increases from 0 to 0.37×10^{12}, 0.76×10^{12}, 1.18×10^{12} and 1.39×10^{12} m⁻¹, approximately 0%, 52%, 70%, 78% and 81% of the total resistance, respectively.

The obtained membranes were used for the static adsorption of Cs⁺ solution (100 mL, 1 mmol L⁻¹, pH 7) for 24 h. With the increased PB contents (0.0125, 0.025, 0.05, 0.075 g), the adsorption uptake of sandwich membranes increases from 0.50 to 0.73, 0.88 and 1.12 mmol m⁻². When the PB content
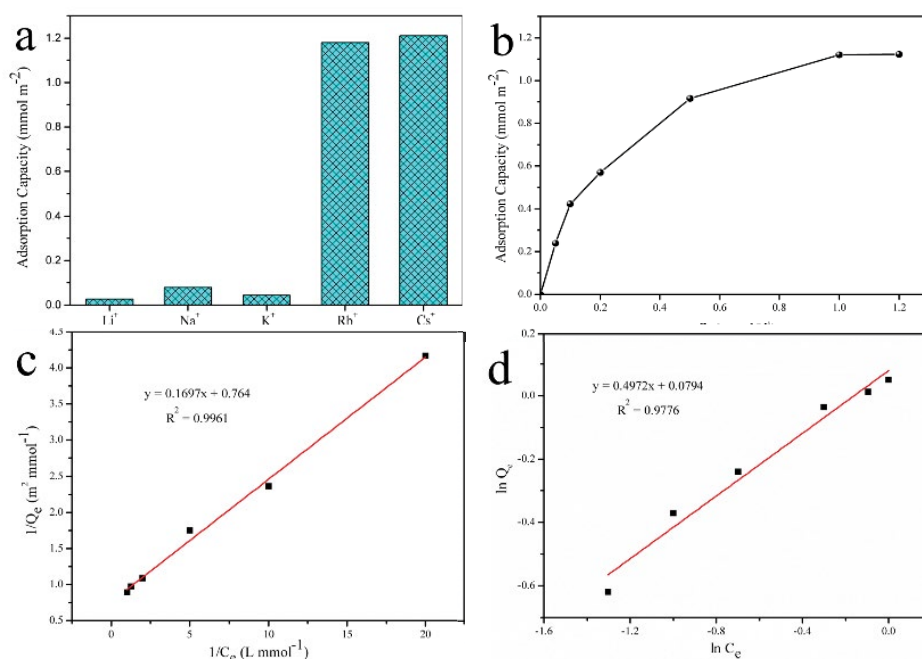
Fig. 3. Effects of membrane fabrication conditions on the flow rate and total resistance. (a) Relative humidity. (b) Polymer concentration. (c) PB contents.

exceeds 0.075 g, the membranes are brittle and not stable. Therefore, 0.075 g of PB was used in the following experiments. Under these optimized fabrication conditions (14% polymer, 0.075 g PB, 60% RH), the respective resistances of the surface layer, the PB layer and the PTFE layer of the membranes are 0.21×10^{12}, 1.39×10^{12} and 0.12×10^{12} m^{-1} (approximately 12%, 81%, and 7% of the total resistance), respectively, demonstrating that the PB layer contributes to the main resistance and the surface layer acts as a liquid distributor with low hydrodynamic resistance.

3.3. Static adsorption of the sandwich membranes

Examination of the static adsorption of the sandwich membranes was carried out in 100 mL of mixed alkali solution (containing Cs$^+$, Rb$^+$, Li$^+$, Na$^+$ and K$^+$, 1 mmol/L for each alkali chloride salt) at 25°C for 24 h. Fig. 4a shows that the adsorption uptake of the sandwich membranes is in the order of Cs$^+$ > Rb$^+$ > Na$^+$ > K$^+$ > Li$^+$, and the selectivity of Cs$^+$ over Li$^+$, Na$^+$ and K$^+$ is 44.31, 15.38 and 27.33, respectively. The adsorption uptake values for Cs$^+$ and Rb$^+$ are 1.21 and 1.18 mmol m^{-2}, respectively due to the similar ion radius. The adsorption uptake of each layer was also determined, respectively. It was found that the PTFE substrate does not adsorb the alkali cations. The PVDF-g-CA layer shows a maximum adsorption capacity of 0.23 mmol m^{-2} (25°C, pH = 7) for Cs$^+$, and the selectivity of Cs$^+$ vs. Li$^+$, Na$^+$ and K$^+$ is 8.46, 3.68 and 3.23, respectively. The maximum adsorption capacity of PB powder for cesium is 0.89 mmol m^{-2} (25°C, pH = 7), and the selectivity of Cs$^+$ vs. Li$^+$, Na$^+$ and K$^+$ is 41.76, 23.67 and 35.50, respectively. From these values, it can be deduced that the PB layer mainly contributes to the adsorption performance of Cs$^+$ in the sandwich membranes.

The selective adsorption of Cs$^+$ by the sandwich membranes can be ascribed to two reasons: (1) PB possesses many lattice defect sites (vacant sites of [Fe(CN)$_6$]$^{4-}$) filled with coordinated and crystal water molecules to form hydrophilic spaces, in which the hydrated metal ions prefer to be absorbed [33]. The hydrated ionic radii of Cs$^+$ and Rb$^+$ are smaller than those of K$^+$, Na$^+$ and Li$^+$, thus favoring adsorption. (2) CA possesses catechol groups, and the phenolic protons can exchange with alkali ions and form phenolates: R–OH + M$^+$ → R–OM + H$^+$. When the hydrated metal ions interact with the hydroxyl of CA, the small hydration energy of Cs$^+$ favors adsorption [35]. Therefore, adsorption is dominated by hydration effects, and the less hydrated ions always prefer adsorption, following the lyotropic series of Cs$^+$ > Rb$^+$ > K$^+$ > Na$^+$ > Li$^+$ [18,36,37].

The static adsorption isotherms of the membranes were determined in 100 mL of Cs$^+$ solution at 25°C for 24 h. Fig. 4b shows that the adsorption capacity increases with increasing
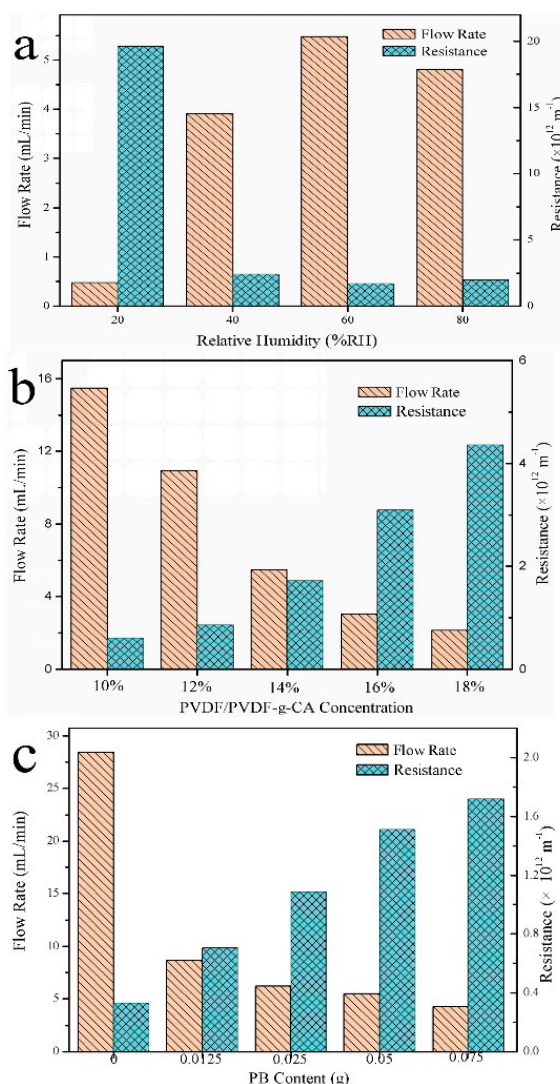
Fig. 4. Static adsorption of membranes. (a) Adsorption uptake for various alkali metal ions. (b) Adsorption isotherm of Cs$^+$. (c) Linear fitted curve of Langmuir model. (d) Linear fitted curve of Freundlich model.

equilibrium concentrations and then approaches a plateau (1.21 mmol m^{-2}, 10.77 mg g^{-1}), which is 1.23 times that of the MMMs (0.98 mmol m^{-2}). To explore the adsorption mechanism, the isotherm results were fitted against the Langmuir and Freundlich models (Table 1). Figs. 4c and d show that the Langmuir adsorption model provides a more satisfactory fitting (R^2 = 0.996) with a maximum adsorption capacity

Table 1
Linear fitting coefficients of adsorption models

	$1/Q_m$	$1/(bQ_m)$	R^2	Q_m (mmol/m^2)	b
Langmuir isotherm					
	0.764	0.1697	0.9961	1.309	4.5017
Freundlich isotherm	$\lg k_F$	$1/a$	R^2	k_F	a
	0.0794	0.4972	0.9776	1.201	2.011

Table 2
Comparison of Cs ion absorbents

Adsorbent	Adsorption capacity (mg g^{-1})	Ref.
Nickel hexacyanoferrate-walnut shell	4.94	[7]
Sericite	6.68	[39]
Brewery's waste biomass	10.1	[40]
Moss	6	[41]
PVDF-g-CA/PB/PTFE membrane	10.77	This work
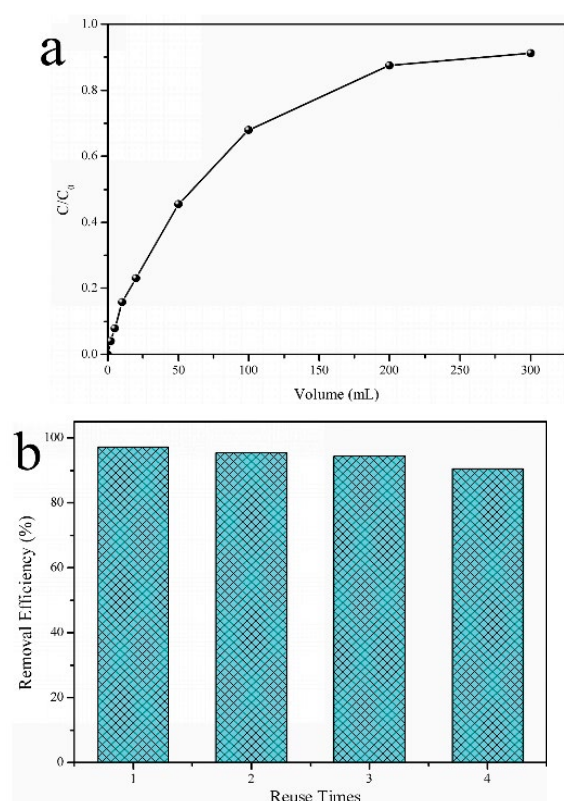
Fig. 5. (a) Breakthrough curve of Cs$^+$ solution. (b) Reuse of membranes.

(Q_m) of 1.21 mmol m^{-2}, indicating the ion exchange adsorption nature [38]. The comparison with other adsorbents for Cs$^+$ is given in Table 2. It can be seen that PVDF-g-CA/PB/PTFE membrane showed higher adsorption capacity than the nickel hexacyanoferrate-walnut shell, sericite, waste biomass, etc.

3.4. Dynamic adsorption and reuse of the membranes

The dynamic adsorption was conducted by filtering 300 mL of 0.05 mmol/L Cs$^+$ solution through the membranes (Φ = 50 mm, membrane volume of 7.85 × 10^{-7} m^3) at a flow rate of 9.33 mL/min. The breakthrough curve is shown in Fig. 5a. It can be seen that c/c_0 increases rapidly in the initial stage (v < 50 mL) and then rises slowly (v > 50 mL).

The breakthrough volume (c/c_0 = 0.1) and saturation volume (c/c_0 = 0.8) are 8 and 150 mL, approximately 10 and 190 times the membrane volume, respectively. The dynamic adsorption capacity (DC) of the membranes at 0.1c_0 and 0.8c_0 can be calculated as Eq. (4):

$$DC = \frac{\int_0^v (c_0 - c) dv}{w_0} \tag{4}$$

The breakthrough capacity (DC$_{0.1}$) is 0.25 mmol g^{-1}, and the saturated capacity (DC$_{0.8}$) is 1.08 mmol g^{-1}, respectively. To study the reusability of the membranes, the saturated membranes were eluted with 10 mL of mixed solution of 0.1 mol/L NH$_4$Cl and 0.01 mol/L HCl at a flow rate of 0.2 mL/min and then reused in dynamic adsorption of Cs$^+$ solution (1 mmol/L), and the adsorption/elution cycle was repeated four times. Fig. 5b shows that the removal efficiency in the four cycles is 97.23%, 95.45%, 94.44% and 90.50%, indicating good reusability of membranes.

4. Conclusions

PVDF-g-CA/PB/polytetrafluoroethylene sandwich membranes were fabricated by the filtration/VIPS method for the intensified adsorption of Cs$^+$. Under optimized fabrication conditions, the maximum adsorption capacity is 1.21 mmol m^{-2} for Cs$^+$, and the selectivity of Cs$^+$ over Li$^+$, Na$^+$ and K$^+$ is 44.31, 15.38 and 27.33. The adsorption isotherm of Cs$^+$ can be well described by the Langmuir model. With the increased polymer concentration and PB contents, the membrane resistance increases, and the PB resistance generally contributes to the main resistance of the membranes. The sandwich membranes exhibit excellent dynamic adsorption performance and reusability, indicating great potential for the adsorption of Cs$^+$.

Acknowledgments

References

[1] T. Sangvanich, V. Sukwarotwat, R.J. Wiacek, R.M. Grudzien, G.E. Fryxell, R.S. Addleman, C. Timchalk, W. Yantasee, Selective capture of cesium and thallium from natural waters and simulated wastes with copper ferrocyanide functionalized mesoporous silica, J. Hazard. Mater., 182 (2010) 225–231.

[2] J.R. Monnier, J.L.S. Jr, R.L. Minga, Stability and distribution of cesium in Cs-promoted silver catalysts used for butadiene epoxidation, J. Catal., 226 (2004) 401–409.

[3] W.J. Yang, S.M. Liu, Y.J. Li, Y.J. Huang, X.S. Luo, Process analysis of Rb$^+$ and Cs$^+$ adsorption from Salt Lake brine by ammonium molybdophosphate composite material, Adv. Mater. Res., 785–786 (2013) 812–816.

[4] R. Kamaraj, S. Vasudevan, Evaluation of electrocoagulation process for the removal of strontium and cesium from aqueous solution, Chem. Eng. Res. Des., 93 (2015) 522–530.

[5] J.L. Nelson, G.J. Alkire, B.W. Mercer, Inorganic ion exchange separation of cesium from purex-type high-level radioactive wastes, Ind. Eng. Chem., 3 (1963) 143–148.

[6] A. Nilchi, R. Saberi, M. Moradi, H. Azizpour, R. Zarghami, Adsorption of cesium on copper hexacyanoferrate–PAN

composite ion exchanger from aqueous solution, Chem. Eng. J., 172 (2011) 572–580.

[7] D. Ding, Y. Zhao, S. Yang, W. Shi, Z. Zhang, Z. Lei, Y. Yang, Adsorption of cesium from aqueous solution using agricultural residue – walnut shell: equilibrium, kinetic and thermodynamic modeling studies, Water Res., 47 (2013) 2563–2571.

[8] A.D. Ebner, J.A. Ritter, J.D. Navratil, Adsorption of cesium, strontium, and cobalt ions on magnetite and a magnetite–silica composite, Ind. Eng. Chem. Res., 40 (2001) 1615–1623.

[9] K. Volchek, M.Y. Miah, W. Kuang, Z. Demaleki, F.H. Tezel, Adsorption of cesium on cement mortar from aqueous solutions, J. Hazard. Mater., 194 (2011) 331–337.

[10] Camille Dumat, A. Hervé Quiquampoix, S. Staunton, Adsorption of cesium by synthetic clay–organic matter complexes: effect of the nature of organic polymers, Environ. Sci. Technol., 34 (2000) 2985–2989.

[11] R. Chen, M. Asai, C. Fukushima, M. Ishizaki, M. Kurihara, M. Arisaka, T. Nankawa, M. Watanabe, T. Kawamoto, H. Tanaka, Column study on electrochemical separation of cesium ions from wastewater using copper hexacyanoferrate film, J. Radioanal. Nucl. Chem., 303 (2015) 1491–1495.

[12] S.K. Samanta, M. Ramaswamy, B.M. Misra, Studies on cesium uptake by phenolic resins, Sep. Sci., 27 (1992) 255–267.

[13] A.W. Loven, H.C. Thomas, Adsorption studies on clay minerals: ion-exchange properties of natural and thermally altered montmorillonite, Soil Sci. Soc. Am. J., 29 (1965) 627–651.

[14] D. Banerjee, M.A. Rao, P.K. Wattal, Separation and recovery of Cs from high active waste simulant using resorcinol formaldehyde polycondensate resin: batch and column studies, Sep. Sci. Technol., 48 (2013) 133–139.

[15] T. Arun, R.J. Joseyphus, Prussian blue modified Fe_3O_4 nano-particles for Cs detoxification, J. Mater. Sci., 49 (2014) 7014–7022.

[16] M. Ishizaki, S. Akiba, A. Ohtani, Y. Hoshi, K. Ono, M. Matsuba, T. Togashi, K. Kananizuka, M. Sakamoto, A. Takahashi, Proton-exchange mechanism of specific Cs^+ adsorption via lattice defect sites of Prussian blue filled with coordination and crystallization water molecules, Dalton Trans., 42 (2013) 16049–16055.

[17] A.K. Vipin, B. Hu, B. Fugetsu, Prussian blue caged in alginate/calcium beads as adsorbents for removal of cesium ions from contaminated water, J. Hazard. Mater., 258–259 (2013) 93–101.

[18] Z. Jia, X. Cheng, Y. Guo, L. Tu, In-situ preparation of iron(III) hexacyanoferrate nano-layer on polyacrylonitrile membranes for cesium adsorption from aqueous solutions, Chem. Eng. J., 325 (2017) 513–520.

[19] L. Lin, A. Wang, M. Dong, Y. Zhang, B. He, H. Li, Sulfur removal from fuel using zeolites/polyimide mixed matrix membrane adsorbents, J. Hazard. Mater., 203 (2012) 204–212.

[20] R.J. Gohari, W.J. Lau, T. Matsuura, E. Halakoo, A.F. Ismail, Adsorptive removal of Pb(II) from aqueous solution by novel PES/HMO ultrafiltration mixed matrix membrane, Sep. Purif. Technol., 120 (2013) 59–68.

[21] Z. Jia, M. Jiang, G. Wu, Amino-MIL-53(Al) sandwich-structure membranes for adsorption of p-nitrophenol from aqueous solutions, Chem. Eng. J., 307 (2016) 283–290.

[22] Y. Guo, Z. Jia, Novel sandwich structure adsorptive membranes for removal of 4-nitrotoluene from water, J. Hazard. Mater., 317 (2016) 295–302.

[23] S.A. Pervin, A.A. Prabu, K.J. Kim, T.L. Yong, Preparation and evaluation of poly(vinylidene fluoride)-sulfonated poly (1,4-phenylene sulfide) based membranes with improved hydrophilicity, Macromol. Res., 23 (2015) 86–93.

[24] Z. Jia, Synthesis of Prussian Blue nanocrystals with metal complexes as precursors: quantitative calculations of species distribution and its effects on particles size, Colloids Surf., A, 389 (2011) 144–148.

[25] S. Hao, Y. Geng, Z. Jia, UV pre-activation/thermal initiated grafting of caffeic acid on PVDF for preparation of adsorptive membranes for cesium, React. Funct. Polym., 132 (2018) 120–126.

[26] J.T. Jung, J.F. Kim, H.H. Wang, E.D. Nicolo, E. Drioli, Y.M. Lee, Understanding the non-solvent induced phase separation (NIPS) effect during the fabrication of microporous PVDF membranes via thermally induced phase separation (TIPS), J. Membr. Sci., 514 (2016) 250–263.

[27] D.M. Wang, J.Y. Lai, Recent advances in preparation and morphology control of polymeric membranes formed by nonsolvent induced phase separation, Curr. Opin. Chem. Eng., 2 (2013) 229–237.

[28] J. Ghasemi, S. Saaidpour, Quantitative structure-property relationship study of n-octanol-water partition coefficients of some of diverse drugs using multiple linear regression, Anal. Chim. Acta, 604 (2007) 99–106.

[29] Z. Jia, G. Sun, Preparation of prussian blue nanoparticles with single precursor, Colloids Surf., A, 302 (2007) 326–329.

[30] Q. Gu, Z. Jia, T. Zhen, Preparation of quaternized poly(vinylidene fluoride) membrane by surface photografting and its anti-fouling performance for alkaline proteins, Desalination, 317 (2013) 175–183.

[31] H.A. Tsai, J.H. Lin, D.M. Wang, K.R. Lee, J.Y. Lai, Effect of vapor-induced phase separation on the morphology and separation performance of polysulfone hollow fiber membranes, Desalination, 200 (2006) 247–249.

[32] H.C. Park, Y.P. Kim, H.Y. Kim, S.K. Yong, Membrane formation by water vapor induced phase inversion, J. Membr. Sci., 156 (1999) 169–178.

[33] M.L.A. Park, M. Soo, J.K. Kim, Breath figure patterns prepared by spin coating in a dry environment, Langmuir, 13 (2004) 5347–5352.

[34] B. Tansel, W.Y. Bao, I.N. Tansel, Characterization of fouling kinetics in ultrafiltration systems by resistances in series model, Desalination, 129 (2000) 7–14.

[35] S.K. Samanta, B.M. Misra, Ion exchange selectivity of a resorcinol-formaldehyde polycondensate resin for cesium in relation to other alkali metal ions, Solvent Extr. Ion Exch., 13 (1995) 575–589.

[36] E.R.N. Jr, Phenomenological theory of ion solvation. effective radii of hydrated ions, Biochim. Biophys. Acta, 63 (1959) 566–567.

[37] Z.H. Yang, L. Yang, Y.Q. Ding, S.D. Zhang, A.Z. Cui, Study of separation of Cs and Rb with precipitation process, J. Nucl. Radiochem., 26 (2004) 95–98.

[38] B. Ernst, J. Bodmann, D.P. Dick, Y.P. Dick, An adsorption isotherm from a micro-state model, Adsorption, 10 (2005) 277–286.

[39] J.O. Kim, S.M. Lee, C. Jeon, Adsorption characteristics of sericite for cesium ions from an aqueous solution, Chem. Eng. Res. Design, 92 (2014) 368–374.

[40] C. Chen, J. Wang, Removal of Pb^{2+}, Ag^+, Cs^+ and Sr^{2+} from aqueous solution by brewery's waste biomass, J. Hazard. Mater., 151 (2008) 65–70.

[41] M.V.B. Krishna, S.V. Rao, J. Arunachalam, M.S. Murali, S. Kumar, V.K. Manchanda, Removal of 137Cs and 90Sr from actual low level radioactive waste solutions using moss as a phyto-sorbent, Separ. Purif. Technol., 38 (2004) 149–161.